THE JOURNAL OF PHYSICAL CHEMISTRY Letters

Letter

pubs.acs.org/JPCL

Four-Terminal Tandem Solar Cells Using $CH_3NH_3PbBr_3$ by Spectrum Splitting

Rui Sheng,[†] Anita W. Y. Ho-Baillie,*[,†] Shujuan Huang,[†] Mark Keevers,[†] Xiaojing Hao,[†] Liangcong Jiang,[‡] Yi-Bing Cheng,[‡] and Martin A. Green[†]

[†]Australian Centre for Advanced Photovoltaics (ACAP), School of Photovoltaic and Renewable Energy Engineering, University of New South Wales, Sydney New South Wales 2052, Australia

[‡]Department of Materials Engineering, Monash University, Melbourne, Victoria 3800, Australia

Supporting Information

ABSTRACT: In this work, the use of a high bandgap perovskite solar cell in a spectrum splitting system is demonstrated. A remarkable energy conversion efficiency of 23.4% is achieved when a $CH_3NH_3PbBr_3$ solar cell is coupled with a 22.7% efficient silicon passivated emitter rear locally diffused solar cell. Relative enhancements of >10% are demonstrated by $CH_3NH_3PbBr_3/CH_3NH_3PbI_3$ and $CH_3NH_3PbBr_3$/multicrystalline-screen-printed-Si spectral splitting systems with tandem efficiencies of 13.4% and 18.8%, respectively. The former is the first demonstration of an all perovskite split spectrum system. The $CH_3NH_3PbBr_3$ cell on a mesoporous structure was fabricated by the vapor-assisted method while the planar $CH_3NH_3PbI_3$ cell was fabricated by the gas-assisted method. This work demonstrates the advantage of the higher voltage output from the high bandgap $CH_3NH_3PbBr_3$ cell and its suitability in a tandem system.

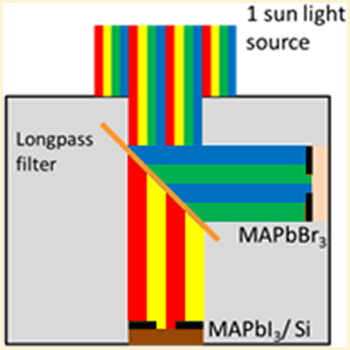

Organic metal halide perovskite solar cell research has experienced a tremendous development over the past three years.[1] There has been a plethora of work focused on increasing the cell energy conversion efficiency[2−8] with the highest of 20.1% being achieved by an intramolecular exchange process (IEP).[8] Attention has been paid to the understanding of fundamental physics and to the study of material properties.[9,10] There is also great interest in integrating perovskite cell with silicon (Si) solar cell.[11−13] Optical splitting is promising for achieving one-sun 28% energy conversion efficiency in a $CH_3NH_3PbI_3$/Si system.[13] The potential of spectrum splitting for ultrahigh performance using Si solar cells is also demonstrated in ref 14, achieving 40% efficient GaInP/GaInAs/Ge and Si spectrum system under 365 suns. Although efforts have been made on developing an ideal 1.6 eV/0.9 eV tandem combination based on Shochley−Queisser limits, the aim of this work is to demonstrate a possibility of using the solar cell with a very large bandgap absorber (2.3 eV in the case of Br perovskite) and high absorption coefficient as the top cell in tandem system. The study of White and et al. demonstrates that the minimum top cell efficiency required to reach 30% tandem efficiency ranges from 22% for a bandgap of 1.5 eV to 14% for a bandgap of 2 eV.[15] Our experimental results demonstrated such a research route of very high bandgap semiconductor materials that can be combined with existing c-Si technology. This work may guide more research interest toward the Br perovskite/Silicon tandem combination, to optimize the monolithic structure, which is more practical and possible to be commercialized in the future.

This work differs from the approach in earlier perovskite/Si split spectrum work. Instead of using a $CH_3NH_3PbI_3$ cell, we demonstrate spectrum splitting systems that utilize a high bandgap (2.3 eV) $CH_3NH_3PbBr_3$ cell in conjunction with a nominal 550 nm spectrum splitter. In addition, an all perovskite $CH_3NH_3PbBr_3/CH_3NH_3PbI_3$ (1.5 eV) split spectrum system is demonstrated for the first time achieving an efficiency of 13.4%. 23.4% conversion efficiency is achieved for the $CH_3NH_3PbBr_3$/Si (1.1 eV) PERL system and remarkably, a relative increase in conversion efficiency of 16% is also achieved by the $CH_3NH_3PbBr_3$/multicrystalline screen-printed (SP) Si spectrum splitting system.

A schematic and a photo of the spectrum splitting system for the measurement of cell conversion efficiencies are shown in Figure 1. A long-pass filter with a nominal cutoff wavelength of 550 nm is used to direct the short wavelength light to the $CH_3NH_3PbBr_3$ cell and the long wavelength light to the $CH_3NH_3PbI_3$ cell or the Si cell. The reflectance, transmittance, and absorption property of the filter at an incident of 45 deg is shown in Figure 1c.

The $CH_3NH_3PbBr_3$ cell was fabricated by the vapor-assisted method,[7] with the structure of Glass/FTO/Compact TiO_2/mesoporous $TiO_2/CH_3NH_3PbBr_3$/Spiro-OMeTAD/Au. The $CH_3NH_3PbI_3$ cell was fabricated by the gas-assisted method.[16] The structure is Glass/FTO/Compact $TiO_2/CH_3NH_3PbI_3$/Spiro-OMeTAD/Au. Two types of Si cells are used. One of

Received: July 26, 2015
Accepted: September 14, 2015
Published: September 14, 2015

DOI: 10.1021/acs.jpclett.5b01608
J. Phys. Chem. Lett. 2015, 6, 3931−3934

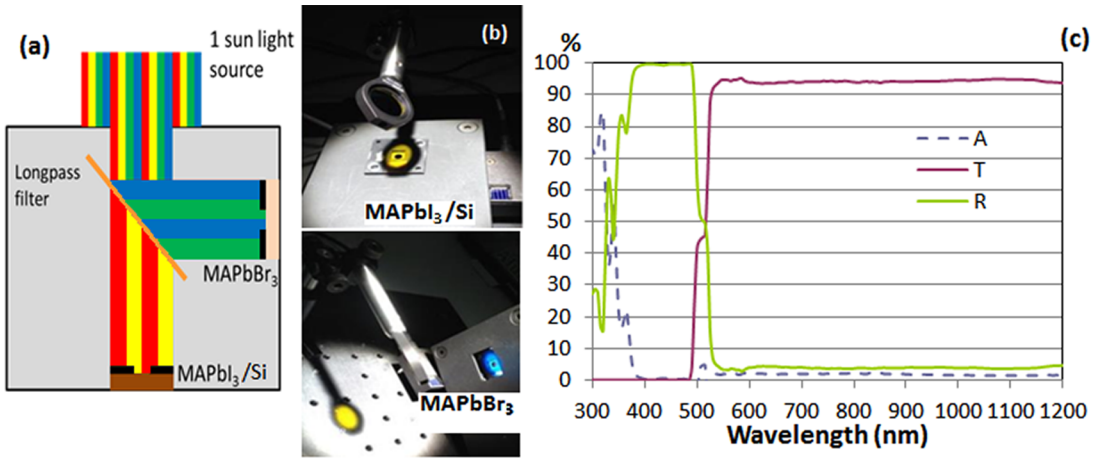

Figure 1. (a) A schematic of the spectrum splitting system setup and (b) a photo of the setup inside the enclosure for the measurement of light current−voltage characteristics. (c) Measured transmittance and reflection and calculated absorption of the FELH0550 long-pass filter at an incident of 45°.

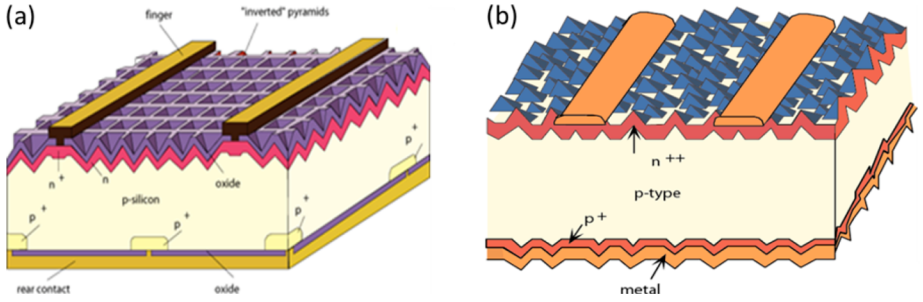

Figure 2. (a) Si PERL and (b) multicrystalline SP Si solar cells used in the spectrum splitting systems.

which is a Si PERL cell while the other is a multicrystalline SP cell (see Figure 2).

The one-sun current density−voltage (J−V) curves and their characteristics measured under 3 V/s reverse scan are summarized in Table 1. The spectral responses (EQE) of the

Table 1. Output Parameters of the Spectral Splitting Systems Using $CH_3NH_3PbBr_3$

	V_{OC} (V)	J_{SC} (mA/cm^2)	FF (%)	Eff. (%)
$CH_3NH_3PbBr_3$ before splitter	1.283	9.5	73	8.8
$CH_3NH_3PbBr_3$ after splitter	1.265	7.2	72	6.5
$CH_3NH_3PbI_3$ before splitter	0.832	20.7	70	12
$CH_3NH_3PbI_3$ after splitter	0.826	12.1	68	6.9
Si PERL before splitter	0.68	42	79	22.7
Si PERL after splitter	0.673	31.6	80	16.9
SP Si before splitter	0.587	34.9	79	16.2
SP Si after splitter	0.578	27.1	79	12.3
$CH_3NH_3PbBr_3$ and $CH_3NH_3PbI_3$ combined				13.4
$CH_3NH_3PbBr_3$ and Si PERL combined				23.4
$CH_3NH_3PbBr_3$ and SP Si combined				18.8

$CH_3NH_3PbBr_3$, $CH_3NH_3PbI_3$, Si PERL, and SP Si cells measured before and after spectral splitting are shown in Figure 3. There is stronger hysteresis in the J−V characteristics of $CH_3NH_3PbI_3$ compared to $CH_3NH_3PbBr_3$ (see Figure S1, Tables S1 and S2 in the Supporting Information),

As evident from Figure 3b (dotted versus solid green curves), the $CH_3NH_3PbBr_3$ cell absorbed less than expexted in the ultraviolet (UV) range and near the band-edgeafter spectral splitting. The former is due to the absorption of UV light by the spectral splitter, as shown by the green curve in Figure 1c, while the latter is due to the lower actual cutoff wavelength (<550 nm) of the splitter at an incident of 45 deg. The $CH_3NH_3PbI_3$ and Si cells also suffered losses due to parasitic absorption by the spectral splitter after the cutoff wavelength.

Nevertheless, the use of the $CH_3NH_3PbBr_3$ cell in the spectral splitting system boosts the performance of the $CH_3NH_3PbI_3$ cell by 11% relative and Si PERL cell by 3% relative. An even higher enhancement of 16% relative or 2.6% absolute was achieved in the $CH_3NH_3PbBr_3$/SP-Si system. This demonstrates the advantage of using a higher bandgap perovskite cell with a Si cell even though the 2.3 eV/1.1 eV bandgap combination is less than the ideal 1.6 eV/0.9 eV binary tandem combination as determined by the detailed balance model with cell efficiencies at the Shockley−Queisser limits.[17] This is because our tandem system takes advantage of the higher voltage output by the $CH_3NH_3PbBr_3$ cell, although its efficiency is far from the theoretical limit (~16%) for a 2.3 eV cell, without diverting too much light from the Si cell that has excellent spectral response to a wider wavelength range (e.g., in excess of 90% for red and near-infrared light).

Furthermore, a higher relative efficiency improvement is achieved when a commercial-type screen-printed soar cell is used in the Perovskite/Si spectral splitting tandem compared to the case when a laboratory developed PERL cell is used (see Table 1 and Table S3). This shows the selection of screen-printed silicon and $CH_3NH_3PbBr_3$ would be a logical choice also from an economic point of view. As the performance of perovskite cells improves, lower bandgap (closer to 1.6 eV)

DOI: 10.1021/acs.jpclett.5b01608
J. Phys. Chem. Lett. 2015, 6, 3931−3934

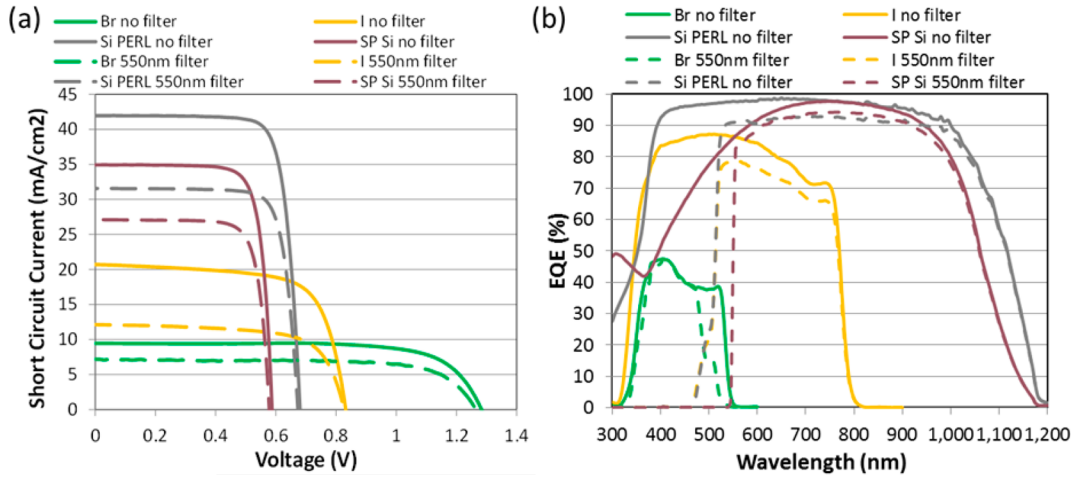

Figure 3. (a) $J-V$ curves and (b) EQE of the $CH_3NH_3PbBr_3$ (green); $CH_3NH_3PbI_3$ (yellow); Si PERL (gray); and SP Si cells (violet) measured before and after spectral splitting.

cells will be effective in a tandem system. For future work in improving spectral splitting systems, better filter designs including the option of short pass filter will also be required using improved optical element with more accurately defined cutoff wavelength, low UV absorption, and close to unity transmittance.

We have demonstrated a spectrum splitting system that capitalizes on higher bandgap inorganic metal halide perovskite solar cell. . An all-perovskite $CH_3NH_3PbBr_3/CH_3NH_3PbI_3$ (1.5 eV) split spectrum system is also demonstrated for the first time. The use of $CH_3NH_3PbBr_3$ cell in a spectral splitting system boosts the performance of the $CH_3NH_3PbI_3$ cell by 11% relative, Si PERL cell by 3% relative, and SP cell by 16% relative resulting in tandem efficiencies of 13.4%, 23.4%, and 18.8%, respectively. Remarkable energy conversion efficiencies are achieved in the $CH_3NH_3PbBr_3$ /Si systems despite the less than ideal 2.3 eV/1.1 eV bandgap combination. This is due to the high voltage output by the $CH_3NH_3PbBr_3$ without diverting too much light from the Si cell that has excellent spectral response to a wide range of wavelength.

As the performance of perovskite cells improves, lower bandgap (closer to 1.6 eV) cells will be effective in a tandem system with $CH_3NH_3PbBr_3$. However, given the relatively higher bandgap and voltage output of $CH_3NH_3PbBr_3$, the future of using $CH_3NH_3PbBr_3$ with screen printed silicon appears promising. Further work to improve the performance of the spectral splitting system will involve the use of optical elements with close to unity reflectance and transmittance and better defined cut-offs optimized for improved perovskite solar cells and high-performance Si cells in binary or even higher order tandem configurations.

EXPERIMENTAL METHODS

$CH_3NH_3PbBr_3$ cell was fabricated by the vapor-assisted method.[7] FTO glass was patterned with 2 M HCl and zinc powder. Substrates were then cleaned in 2% Hallmanex detergent, acetone, and isopropanol in ultrasonic bath for 10 min in each cleaning agent followed by UVO treatment for 10 min. The compact TiO_2 layer was deposited by spin-coating a mildly acidic solution of titanium isopropoxide in ethanol at 2000 rpm for 60 s followed by annealing at 150 °C for 10 min and then 500 °C for 30 min. The mp-TiO_2 layer composed of 20 nm-sized particles was deposited by spin-coating at 2000 rpm for 60 s using a commercial TiO_2 paste (Dyesol 18NRT, Dyesol) diluted in ethanol (2:7, weight ratio). After being dried at 125 °C, the TiO_2 film was heated to 500 °C, annealed at this temperature for 30 min, and gradually cooled to room temperature. For deposition of $CH_3NH_3PbBr_3$ film, first, $PbBr_2$ solution in DMF with a concentration of 1 M was spin-coated on the mp-TiO_2 at 2000 rpm for 60 s. After annealing at 70 °C for 30 min, the film was treated by CH_3NH_3Br vapor at 175 °C for 10 min in a closed glass Petri-dish with CH_3NH_3Br powder surrounded on a hot plate in a glovebox, then rinsed in isopropanol at room temperature. HTM was then deposited by spin-coating at 2000 rpm for 60 s. The solution was prepared by dissolving 72.3 mg (2,2′,7,7′-tetrakis(*N*,*N*-di-*p*-methoxyphenyl-amine)-9,9′-spirobifluorene) (spiro-MeOTAD), 28.8 μL 4- *tert*-butylpyridine (4-TBP), and 17.5 μL of a stock solution of 520 mg/mL lithium bis(trifluoromethane)sulfonimide (LiTFSI) in acetonitrile in 1 mL Chlorobenzene. Finally, 100 nm gold contacts were thermally evaporated to form the complete device.

The $CH_3NH_3PbI_3$ cell was fabricated by the gas-assisted method[16] using pyrolysis spray deposit and a TiO_2 dense blocking layer on the clean FTO glass at 450 °C. The solution was mixed by bis(isopropoxide)-bis(acerylacetonate)titanium-(IV) solution and ethanol with a volume ratio of 1:39. A 25 μL 45% $CH_3NH_3PbI_3$ DMF solution, prepared from PbI_2 and CH_3NH_3I in a molar ratio of 1:1, was spread on a spin-coater, and a 40 psi dry N_2 gas stream was blown over the film during spinning at 6500 rpm in 2 s after the spin-coating commenced. The films were then annealed at 100 °C for 10 min, and then cooled to room temperature. A 25 μL Spiro-OMeTAD solution, prepared by dissolving 41.6 mg spiro-OMeTAD, 7.5 μL of a stock solution of 520 mg/mL lithium bis-(trifluoromethylsulfonyl)imide in acetonitrile, and 16.9 μL 4-*tert*-butylpyridine in 0.5 mL chlorobenzene was coated on the perovskite film by spin-coating at 3000 rpm for 30 s. A 100 nm gold contact was deposited by thermal evaporation to form the complete device.

The current density−voltage ($J-V$) measurements were performed using an IV5 solar cell I−V testing system from PV measurements, Inc. (using a Keithley 2400 source meter) under illumination power of 100 mW/cm^2 by an AM1.5G solar simulator (Oriel model 94023A). Cells were arranged in spectral a splitting system as illustrated in Figure 1. The

DOI: 10.1021/acs.jpclett.5b01608
J. Phys. Chem. Lett. 2015, 6, 3931−3934

enclosure aperture is 3.5 cm^2. The cell areas measured are 0.045 cm^2, 0.159 cm^2, 1 cm^2, and 1.62 cm^2 for the $CH_3NH_3PbBr_3$, $CH_3NH_3PbI_3$, Si PERL, and SP Si cells, respectively.

A QE-X7 system by PV measurements, Inc. was used to measure the EQE of the cells. Under full computer control, light from a 65 W xenon arc lamp was focused through a monochromator in the 300−1400 nm wavelength range onto the photovoltaic cell under test. The monochromator was incremented through the spectrum to generate the EQE of the cells before and after applying the spectral splitting filter.

Reflectance (R) and transmittance (T) of the filter were measured using a PerkinElmer UV−vis−NIR spectrophotometer at 45 deg incident. For the reflectance measurement, the universal reflectance accessory is used.

■ ASSOCIATED CONTENT

Supporting Information

The Supporting Information is available free of charge on the ACS Publications website at DOI: 10.1021/acs.jpclett.5b01608.

J−V curves and hysteresis of $CH_3NH_3PbI_3$ and $CH_3NH_3PbBr_3$ cells before and after spectral splitting; of $CH_3NH_3PbBr_3$ and $CH_3NH_3PbI_3$ cells before and after spectral splitting; performance of $CH_3NH_3PbI_3$/Si cell via various spectral splitting arrangements (PDF)

■ AUTHOR INFORMATION

Corresponding Author

*E-mail: a.ho-baillie@unsw.edu.au.

Notes

The authors declare no competing financial interest.

■ ACKNOWLEDGMENTS

The Australian Centre for Advanced Photovoltaics (ACAP) encompasses the Australian-based activities of the Australia−US Institute for Advanced Photovoltaics (AUSIAPV) and is supported by the Australian Government through the Australian Renewable Energy Agency (ARENA). This work is part of the ARENA Project 2014/RND075. We thank Dr. Ly Mai and Dr. Hamid Mehrvarz for their assistance in supplying screen-printed multicrystalline and PERL Si solar cells.

■ REFERENCES

(1) Green, M. A.; Ho-Baillie, A.; Snaith, H. J. The Emergence of Perovskite Solar Cells. *Nat. Photonics* **2014**, *8* (7), 506−514.

(2) Burschka, J.; Pellet, N.; Moon, S.-J.; Humphry-Baker, R.; Gao, P.; Nazeeruddin, M. K.; Gratzel, M. Sequential Deposition as a Route to High-performance Perovskite-sensitized Solar Cells. *Nature* **2013**, *499* (7458), 316−319.

(3) Liu, M.; Johnston, M. B.; Snaith, H. J. Efficient Planar Heterojunction Perovskite Solar Cells by Vapour Deposition. *Nature* **2013**, *501* (7467), 395−398.

(4) Chen, Q.; Zhou, H.; Hong, Z.; Luo, S.; Duan, H.-S.; Wang, H.-H.; Liu, Y.; Li, G.; Yang, Y. Planar Heterojunction Perovskite Solar Cells via Vapor-Assisted Solution Process. *J. Am. Chem. Soc.* **2014**, *136* (2), 622−625.

(5) Jeon, N. J.; Noh, J. H.; Yang, W. S.; Kim, Y. C.; Ryu, S.; Seo, J.; Seok, S. I. Compositional Engineering of Perovskite Materials for High-performance Solar Cells. *Nature* **2015**, *517* (7535), 476−480.

(6) Heo, J. H.; Song, D. H.; Im, S. H. Planar CH3NH3PbBr3 Hybrid Solar Cells with 10.4% Power Conversion Efficiency, Fabricated by Controlled Crystallization in the Spin-Coating Process. *Adv. Mater.* **2014**, *26* (48), 8179−8183.

(7) Sheng, R.; Ho-Baillie, A.; Huang, S.; Chen, S.; Wen, X.; Hao, X.; Green, M. A. Methylammonium Lead Bromide Perovskite-Based Solar Cells by Vapor-Assisted Deposition. *J. Phys. Chem. C* **2015**, *119* (7), 3545−3549.

(8) Yang, W. S.; Noh, J. H.; Jeon, N. J.; Kim, Y. C.; Ryu, S.; Seo, J.; Seok, S. I. High-performance Photovoltaic Perovskite Layers Fabricated through Intramolecular Exchange. *Science* **2015**, *348* (6240), 1234−1237.

(9) Wen, X.; Sheng, R.; Ho-Baillie, A. W. Y.; Benda, A.; Woo, S.; Ma, Q.; Huang, S.; Green, M. A. Morphology and Carrier Extraction Study of Organic−Inorganic Metal Halide Perovskite by One- and Two-Photon Fluorescence Microscopy. *J. Phys. Chem. Lett.* **2014**, *5* (21), 3849−3853.

(10) Jiang, Y.; Green, M. A.; Sheng, R.; Ho-Baillie, A. Room Temperature Optical Properties of Organic−inorganic Lead Halide Perovskites. *Sol. Energy Mater. Sol. Cells* **2015**, *137* (0), 253−257.

(11) Mailoa, J. P.; Bailie, C. D.; Johlin, E. C.; Hoke, E. T.; Akey, A. J.; Nguyen, W. H.; McGehee, M. D.; Buonassisi, T. A 2-terminal Perovskite/silicon Multijunction Solar Cell Enabled by a Silicon Tunnel Junction. *Appl. Phys. Lett.* **2015**, *106* (12), 121105.

(12) Loper, P.; Moon, S.-J.; Martin de Nicolas, S.; Niesen, B.; Ledinsky, M.; Nicolay, S.; Bailat, J.; Yum, J.-H.; De Wolf, S.; Ballif, C. Organic-inorganic Halide Perovskite/crystalline Silicon Four-terminal Tandem Solar Cells. *Phys. Chem. Chem. Phys.* **2015**, *17* (3), 1619−1629.

(13) Uzu, H.; Ichikawa, M.; Hino, M.; Nakano, K.; Meguro, T.; Hernández, J. L.; Kim, H.-S.; Park, N.-G.; Yamamoto, K. High Efficiency Solar Cells Combining a Perovskite and a Silicon Heterojunction Solar Cells via an Optical Splitting System. *Appl. Phys. Lett.* **2015**, *106* (1), 013506.

(14) Green, M. A.; Keevers, M. J.; Thomas, I.; Lasich, J. B.; Emery, K.; King, R. R. 40% Efficient Sunlight to Electricity Conversion. *Prog. Photovoltaics* **2015**, *23* (6), 685−691.

(15) White, T. P.; Lal, N. N.; Catchpole, K. R. Tandem Solar Cells Based on High-Efficiency c-Si Bottom Cells: Top Cell Requirements for > 30% Efficiency. *Photovoltaics, IEEE Journal of* **2014**, *4* (1), 208−214.

(16) Huang, F.; Dkhissi, Y.; Huang, W.; Xiao, M.; Benesperi, I.; Rubanov, S.; Zhu, Y.; Lin, X.; Jiang, L.; Zhou, Y.; Gray-Weale, A.; Etheridge, J.; McNeill, C. R.; Caruso, R. A.; Bach, U.; Spiccia, L.; Cheng, Y.-B. Gas-assisted Preparation of Lead Iodide Perovskite Films Consisting of a Monolayer of Single Crystalline Grains for High Efficiency Planar Solar Cells. *Nano Energy* **2014**, *10* (0), 10−18.

(17) Bremner, S. P.; Yi, C.; I. Al-Mansouri, A. Ho-Baillie, Green, M. A. General Design Considerations for Making Optimal Use of New Photovoltaic Materials. In *Proceedings of the 42nd IEEE PVSC*, June 14−19, 2015, New Orleans, LA.

■ NOTE ADDED AFTER ASAP PUBLICATION

This paper was published ASAP on September 17, 2015. Figure 1 and the abstract graphic were updated. The revised paper was reposted on September 22, 2015.

DOI: 10.1021/acs.jpclett.5b01608
J. Phys. Chem. Lett. 2015, 6, 3931−3934